ELSEVIER

Polymer 42 (2001) 7153–7160

polymer

www.elsevier.nl/locate/polymer

Deformation of undrawn poly(trimethylene terephthalate) (PTT) fibers

J.S. Grebowicz[a,*], H. Brown[a], H. Chuah[a], J.M. Olvera[a], A. Wasiak[b], P. Sajkiewicz[b], A. Ziabicki[b]

[a]*Shell Chemical Company, Westhollow Technology Center, Houston, TX, USA*
[b]*Polish Academy of Sciences, Institute of Fundamental Technological Research, Warsaw, Poland*

Received 15 October 2000; received in revised form 3 December 2000; accepted 20 December 2000

Abstract

Fibers were obtained by melt spinning of poly(trimethylene terephthalate) with take-up velocities ranging from 500 to 5000 m/min. Deformation behavior was analyzed with the use of a thermo-mechanical analyzer (TMA). Constant force and isostrain experiments were done. The structure of undrawn fibers was analyzed by optical birefringence, density, wide-angle X-ray diffraction (WAXD) and differential scanning calorimetry (DSC).

Complex thermo-mechanical behavior — spontaneous elongation of some samples, thermal shrinkage of others, maxima of shrinkage vs. spinning speed — can be explained by the initial structure of fibers and structural processes accompanying deformation. With increasing take-up speed, molecular orientation and crystallinity of fibers increase. The fibers differ also in their ability to crystallize. Initially amorphous (low-speed-spun) fibers crystallize when heated above glass transition temperature. This effect ("cold crystallization") has been observed in DSC.

Keywords: PTT Poly(trimethyleneterephthalate) fiber; Shrinkage

1. Introduction

It is well known that conditions occurring in the spinning line determine the structure and properties of as-spun fibers [1], and their behavior in further technological operations. In spite of this general knowledge, each time a new polymer or new spinning technology emerges, it becomes necessary to establish "spinning conditions–structure" and "structure–properties" relationships valid for the specific material and the particular technology.

The present paper is devoted to the studies of such relationships for high-speed spinning of poly(trimethylene terephthalate) (PTT), commercialized under the name Corterra®. PTT is a crystallizable polymer, with the chemical structure:

$$-[-(C{=}O)-(C_6H_4)-(C{=}O)-O-CH_2-CH_2-CH_2-O-]_x-$$

that crystallizes in a triclinic unit cell [2–4].

This paper reports studies on the structure and properties of fibers melt-spun at various take-up velocities. Fibers have been characterized by X-ray diffraction, density, birefringence and thermo-mechanical studies.

2. Experimental

Polymer: Corterra® PTT polymer with an intrinsic viscosity of 0.9 dl/g (measured in a 50/50 mixture of methylene chloride and trifluoroacetic acid at 30°C).

Fiber formation: The polymer was processed on the Westhollow Technology Center Fiberline described below. The extrusion temperature was 263°C.

Drying: Two Novatec dryers (one for each extruder below) set at 130°C and measuring less than −60°C dew points are used to dry the polymer. The polymer is air transferred into the extrusion system below. Two more Novatec dryers rest on each extruder and are used to keep the polymer at 130°C.

Extrusion: The extrusion system used consists of dual 1-in., 30:1 *L/D* Hills, Inc. extruders. Additionally, each extruder has venting capabilities. The fiber line was run with either extruder alone to produce homofilaments. A water jacket was used to cool the feed throat section of the extruder. Temperatures were monitored and controlled in four zones along the length of the barrel, and melt temperature was monitored at the tip of the screw.

* Corresponding author. Tel.: +1-281-544-7508; fax: +1-281-544-7803.
E-mail addresses: jsgrebowicz@shellus.com (J.S. Grebowicz), aziab@ippt.gov.pl (A. Ziabicki).

0032-3861/01/$ - see front matter
PII: S0032-3861(01)00047-7

Pressure was set and monitored at the tip of the screw. The monitored pressure was fed back to the computer control system, which automatically maintained melt pressure by adjusting the extruder speed. The molten polymer passes through a matched set of either 2.92 or 4.0 cc/rev Feinpruef melt pumps, which maintain positive volumetric polymer displacement. After having passed through another pressure and melt temperature monitoring zone, the molten polymer passed through distribution plates, a screen pack, and then a 50-hole spinnerette (two positions). These packs are constructed such that each 50-hole bundle was fed by a single extruder/melt pump configuration.

Quenching: Quenching was accomplished through a 6.25-ft, three-zone, cross-flow quench system with Purolator 40-μm diffuser panels. The air temperature was set and controlled by running chilled (or heated) water through a standard air conditioner coil. Air was pulled across the coil with three independent variable-speed fans in a common plenum. The top zone was a 3-in., high-velocity short-gap zone. The second and third zones were 3-ft, low-velocity long-gap zones. The actual air velocity and temperature were monitored in the individual supply plenums for the three zones. Spin finish was applied in this section with a metering jet, driven by Zschimmer and Schwarz finish pumps.

POY: The fibers passed two 0.75-m cold rolls in a reverse "S" configuration, with interlacing applied in-between the two rolls. Typically, the rolls were run faster than the run speed, which was determined by the winder. The speed of the second cold roll was adjusted to give 0.03–0.05 g/denier winding tension, while the first was adjusted to give good tack in the interlacing jet.

Winders: Winding was done with a Barmag SW46SSD high-speed winder, with a speed range of 500–5000 m/min.

3. Measurements

X-ray diffraction patterns from a bunch of parallel fibers were recorded with CuK_α radiation using the image plate as two-dimensional position-sensitive detector. From each intensity distribution, the amorphous halo and crystalline reflections (when applicable) were separated, and their azimuthal dependencies determined. From the azimuthal intensity distribution, $I(\delta)$, the average $\langle \sin^2 \alpha \rangle$ was computed and later the orientation factor was determined.

Crystal orientation was estimated on the basis of the (010) crystallographic plane, one giving equatorial reflection at $2\vartheta = 15.66°$. Using the azimuthal profile of intensity $I(\delta)$ at a constant Bragg angle, ϑ, the following characteristics were computed:

$$\langle \sin^2 \alpha \rangle = \frac{\int_0^{\pi/2} I(\alpha) \sin^3 \alpha \, d\alpha}{\int_0^{\pi/2} I(\alpha) \sin \alpha \, d\alpha} \quad (1)$$

Conversion from the azimuthal angle δ to the angle α was done according to the Polanyi equation:

$$\cos \alpha = \cos \delta \cos \vartheta \quad (2)$$

The orientation factor of the reciprocal vector r^*_{010} was determined according to the definition:

$$f_{hkl} = 1 - \tfrac{3}{2}\langle \sin^2 \alpha_{hkl} \rangle \quad (3)$$

Finally, the approximate value of the orientation factor for the c-axis of the crystal was estimated as:

$$f_c = -2 f_{010} \quad (4)$$

Amorphous orientation was estimated in a similar manner from the azimuthal intensity distribution corresponding to the maximum of the amorphous halo.

Azimuthally averaged intensity distributions were used to compute the degree of crystallinity of the fibers.

Density was measured using a density gradient column filled with the *n*-heptane/CCl_4 mixture. Prior to placement into the column, samples were degassed under vacuum and wetted with the liquid of composition corresponding to the upper part of the column. Readings of the sample positions were taken after a period of time ca 1 h, which was found sufficient for reaching equilibrium. Accuracy of measurements was ± 0.0005 g/cm^3.

Optical properties were determined by means of:
(1) Polarizing interference microscope (designed by M. Pluta), produced by Polish Optical Works (PZO), Warsaw. The fringed field interference at crossed polarizer vs. analyzer was applied. Three orientations of the fiber with respect to polarization planes were used in order to determine independently: birefringence, Δn (fiber oriented at 45° with respect to both polarization planes), and refractive indices parallel ($n_\parallel$) and perpendicular ($n_\perp$) to the fiber axis, measured parallel to either polarization plane (polarizer or analyzer). Fibers were immersed in Cargilles® immersion oil with refractive index $n = 1.515$. Optical retardation was calculated from the shift of the fringe in the corresponding image. Diameter of the fiber was measured at the same point as retardation.
(2) Leitz Orthopan Polarizing Microscope equipped with 25 × oil immersion objective and Leitz 2147 K Tilting Compensator.

The data for which results from both instruments were consistent have been used for further analysis.

Differential scanning calorimetry (DSC) measurements were performed using Perkin–Elmer DSC-7 and TA Instruments DSC. Some measurements were performed at constant length, which was achieved through winding of fibers on a small spool [5], later placed in a DSC pan.

Thermo-mechanical measurements were conducted using a TMA 2940 apparatus, produced by Du Pont Instruments. Measurements were done in the temperature range 30–200°C.

Table 1
Thermo-mechanical behavior of PTT fibers. The effect of spinning speed at constant deformation force, F

Load, (N)	Stress (MPa)	Spinning speed, V_L (m/min)	Shrinkage		T_{trans} (°C)	Elongation			
			T_{beg} (°C)	Shrinkage (%)		Elongation (%)	T_{end} (°C)	Shrinkage rate (μm/m/°C)	Elongation rate (μM/m/°C)
0.001	0.056	500	52	20	61	5	68	13900	2630
		1000	52	39	62	4	67	27600	96
		1500	48	21	57	7	66	14200	5150
		2000	52	47	57	11	65	28100	913
		2500	59	26	62	9	67	17700	8970
		3000	59	11	65	3	81	7690	684
		3500	46	5	49	No elongation; only shrinkage		3600	
		4000	49	8	55			5700	
		4500	62	5	67			2570	
		5000	62	6	66			3780	
0.003	0.168	500	52	11	59	7	67	8360	4930
		1000	52	22	58	4.5	66	16200	11500
		1500	53	48	59	11	67	35400	4560
		2000	45	55	51	16	62	39000	5660
		2500	52	25	57	9	68	16400	5480
		3000	49	9	54	No elongation; only shrinkage		6130	
		3500	58	3	61			1800	
		4000	58	3	70			1230	
		4500	57	6	61			3540	
		5000	62	5	72			220	
0.05	2.76	500	51	Catastrophic elongation at 50°C					
		1000	49						
		1500	52						
		2000	51	No shrinkage		23	61		13200
		2500	53			7	70		2950
		3000	54			0.9	56		173
			56	1.4	64			240	
			64			1.7	85		798
		3500	57	2.5	67	0.5	89	1610	235
		4000	66	1.4	74	No elongation; only shrinkage		906	
		4500	69	3	95			1060	
		5000	65	2.5	78			1110	
0.26	14.4	500	54	No shrinkage		Catastrophic elongation above 50°C			
		1000							
		1500							
		2000							
		2500	55			37	57		102000
		3000	57			28	61		29900
		3500	58			6	63		2840
		4000	57			2	75		415
		4500	56			0.9	68		696
		5000	52			1.2	69		781

4. Results

The present paper is aimed at correlation between macroscopic properties of fibers submitted to thermal treatment (mainly shrinkage), and the structural characteristics of those fibers prior to thermal treatment. Relationships between various structural characteristics will be investigated in a subsequent paper [6].

4.1. Thermo-mechanical studies

Numerical results of thermo-mechanical investigations are summarized in Table 1. It can be seen that in most cases shrinkage of the fibers occurs first when the temperature is elevated. The amount of shrinkage depends upon take-up velocity, V_L.

At relatively low take-up velocities, the higher the velocity, the smaller the shrinkage. This behavior occurs till about 2500 m/min, where shrinkage reaches a maximum. Fibers spun at higher velocities show decrease of shrinkage with increasing take-up velocity. For all spinning speeds, however, the initial temperature at which the fibers start shrinking increases with increasing take-up velocity.

When the temperature is raised above some transition temperature (also dependent upon spinning speed), the process of elongation (deformation) starts. This process is strongly dependent on the load applied to the sample. When the load, F, is small, post-shrinkage elongation is observed only for fibers spun at relatively low spinning speeds: up to 3000 m/min at $F = 0.001$ N (which corresponds to tensile stress of about 0.056 MPa in the filament), and up to 2500 m/min at $F = 0.003$ N (tensile stress ca. 0.168 MPa). (The transition temperature, in those cases, denotes the temperature at which shrinkage reaches saturation.)

The application of higher loads, i.e. when large axial force $F = 0.05$ N (resulting in 2.76 MPa stress), and $F = 0.26$ N (14.4 MPa stress) is applied to the fibers, prevents shrinking, causing elongation of fibers after the temperature reaches ca 50°C. A sufficiently high load causes elongation, starting at temperatures about 50°C and lasting until the break occurs.

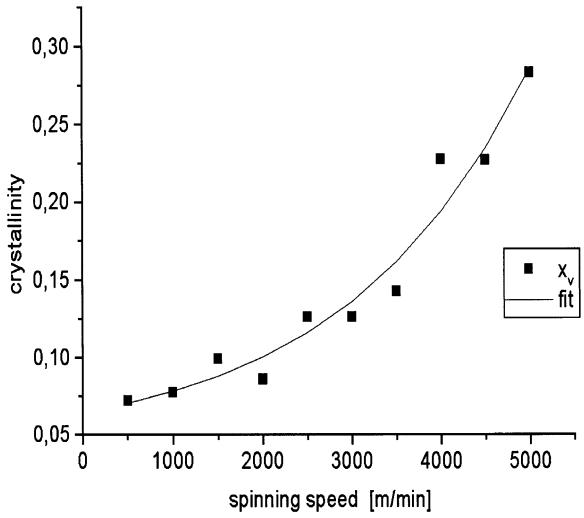

Fig. 1. Crystallinity as a function of spinning speed.

4.2. Density

Table 2 shows the density as a function of spinning speed. The density was then used for calculation of the weight crystallinity, x_w, and volume crystallinity, x_v

$$x_w = \frac{\rho_c}{\rho}\frac{\rho - \rho_a}{\rho_c - \rho_a}; \qquad x_v = \frac{\rho - \rho_a}{\rho_c - \rho_a} \tag{5}$$

where ρ_c and ρ_a are crystal and amorphous density, respectively. Crystallinity was calculated using $\rho_c = 1.4412$ g/cm^3 and $\rho_a = 1.2990$ g/cm^3 as determined previously for an unoriented polymer [7]. Another set of crystallinity values, computed on the basis of $\rho_a = 1.3067$ g/cm^3 [5] is also reported in Table 2. It can be seen from Fig. 1 that crystallinity increases with the spinning velocity.

Table 2
Densities of undrawn PTT fibers and values of crystallinity derived using different sets of crystalline and amorphous density

Spinning speed, V_L (nm/min)	Density, ρ (g/cm^3)	Standard deviation	Crystallinity ($\rho_{cr} = 1.4412$; $\rho_{am} = 1.299$)		Crystallinity ($\rho_{cr} = 1.4412$; $\rho_{am} = 1.3067$)	
			x_v	x_w	x_v	x_w
500	1.30921	0.0022	0.0718	0.079039	0.018662	0.020543
1000	1.30996	0.000431	0.077075	0.084796	0.024238	0.026666
1500	1.31306	0.000435	0.098875	0.108524	0.047286	0.051901
2000	1.31119	0.00043	0.085724	0.094224	0.033383	0.036693
2500	1.31691	0.000262	0.125949	0.137836	0.075911	0.083075
3000	1.3169	0.000526	0.125879	0.137761	0.075836	0.082995
3500	1.31931	0.000538	0.142827	0.156023	0.093755	0.102417
4000	1.33132	0.000975	0.227286	0.246044	0.183048	0.198156
4500	1.33125	0.000893	0.226793	0.245524	0.182528	0.197603
5000	1.33926	0.000241	0.283122	0.304673	0.242082	0.260508

Table 3
Characteristics of molecular and crystal orientation determined from X-ray diffraction diagrams

V_L	$\langle \sin \alpha \rangle^2_{am}$	$f_{\perp,am}$	$f_{c,am}$	$\langle \sin \alpha \rangle^2_{cr}$	f_{010}	$f_{c,cr}$
500	0.693095	−0.03964	0.07928			
1000	0.69503	−0.04255	0.085098			
1500	0.707134	−0.0607	0.1214			
2000	0.71611	−0.07416	0.14832			
2500	0.722395	−0.08359	0.167186			
3000	0.73701	−0.10552	0.211034			
3500	0.73512	−0.10268	0.205368	0.737362	−0.10604	0.212086
4000	0.739309	−0.10896	0.217928	0.97829	−0.46744	0.93487
4500	0.730674	−0.09601	0.19202	0.97209	−0.45814	0.916278
5000	0.727549	−0.09132	0.182648	0.989068	−0.4836	0.9672

4.3. X-ray diffraction (WAXS)

The character of the X-ray diffraction pattern depends on spinning conditions, reflecting changes both in crystallinity and orientation. The reflection at the azimuthal angle of 90° and $2\vartheta \approx 15.7°$ corresponding to the crystallographic plane (010) is visible on the patterns obtained from fibers spun between 3500 and 5000 m/min. It is clear that no crystalline reflections appear on patterns from fibers spun at low speeds. Consequently, X-ray crystallinity and orientation of crystals become measurable for fibers spun at high speeds, starting from 3500 m/min.

Quantitative characteristics determined from the azimuthal intensity distribution of the amorphous halo and for the 010 diffraction maximum are presented in Table 3. It can be seen that amorphous orientation depends on spinning speed. It increases first with an increase of take-up velocity V_L, reaches a flat maximum at speeds between 3000 and 4000 m/min, and slightly decreases for higher speeds. The orientation of the crystalline phase is usually higher, and for fibers spun above 4000 m/min, the orientation factor f_{cr} is very close to unity (almost perfect alignment of crystal *c*-axes with respect to the fiber axis). It should be noted that the reduction of the amorphous orientation at high spinning speeds is accompanied by an increase of (already very high) crystal orientation. Amorphous, f_{am}, and crystal orientation factors, f_{cr}, are plotted as functions of spinning speed in Fig. 2. It is clearly seen that in the range of spinning speeds not exceeding 3000 m/min, crystallinity is rather weak. The abrupt change of this behavior occurs within a narrow range of spinning speeds, and finally at $V_L > 3500$ m/min a saturation of the orientation factor at a high level is observed. This behavior can be explained on the basis of the theory of oriented crystallization, and was observed also in poly(ethylene terephthalate) fibers [2].

4.4. Optical properties

Results of optical investigations are presented in Table 4. They include birefringence and separately measured refractive indices in directions perpendicular, $n_\perp$, and parallel, $n_\parallel$, to the fiber axis. An increase of birefringence with an increase of spinning speed, reaching saturation at high speeds, is evidently visible, and remains in good agreement with X-ray orientation measurements, since birefringence consists of contributions from both amorphous and

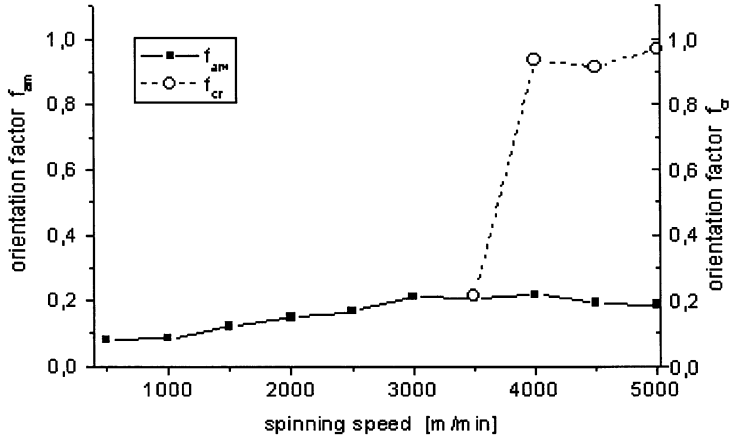

Fig. 2. Amorphous and crystal orientation factors as functions of spinning speed.

Table 4
Optical properties of undrawn PTT fibers

V_L	Δn^a	Δn^b	d (μm)	$n_\perp$	$n_\parallel$	$n_\parallel - n_\perp$	n_{iso}
500	0.008337	0.00721	24.379	1.589567	1.599	0.009433	1.592711
1000	0.012802	0.0126	20.217	1.601482	1.615715	0.014233	1.606226
1500	0.02101	0.0237	20.217	1.597772	1.621453	0.023681	1.605666
2000	0.034495	0.037	20.812	1.592033	1.628582	0.036549	1.604216
2500	0.043083	0.0489	22.001	1.588366	1.62437	0.036004	1.600367
3000	0.05248	0.0533	21.406	1.584068	1.637246	0.053178	1.601794
3500	0.053974	0.0504	22.595	1.587221	1.631526	0.044305	1.601989
4000	0.046306	0.0504	20.217	1.595773	1.639757	0.043984	1.610434
4500	0.054735	0.0499	22.001	1.590266	1.641557	0.051291	1.607363
5000	0.051706	0.0489	20.812	1.595703	1.64523	0.049527	1.612212

[a] Measured by means of PZO interference microscope.
[b] Measured by means of Orthopan polarising microscope.

crystalline orientations. Average "isotropic" refractive index:

$$n_{iso} = \tfrac{1}{3}(n_\parallel + 2n_\perp) \quad (6)$$

corresponds to the crystallinity and correlates with the density of the polymer.

4.5. Differential scanning calorimetry

Typical DSC scans for the melting of constrained and unconstrained fibers are shown in Figs. 3 and 4. Melting temperatures obtained from calorimetric measurements are presented in Table 5. Two transitions are common for all investigated fibers: glass transition and melting. In the case of fibers spun at low speeds, glass transition is followed additionally by cold crystallization. Both the spinning speed and constraints applied to the sample during calorimetric studies show influence on the measured characteristics.

4.6. The effect of spinning rate

The biggest effect of the spinning speed concerns crystallinity. It is seen that the crystallinity of as-spun samples obtained by subtraction of the heat of cold crystallization from the heat of melting increases with spinning rate. For fibers spun at the speed of 500 m/min the initial crystallinity is about 20% and increases to ca. 45% for fibers spun at 5000 m/min.

Cold crystallization is relatively large in fibers with low initial crystallinity ($\Delta x_v = 20\%$ for spinning speed 500 m/min), and disappears in fibers spun at high speeds with high initial crystallinity. The temperature of glass transition increases with take-up velocity, while the peak temperature of the cold crystallization shows a minimum at moderate spinning speeds.

Melting of the crystalline phase occurs at temperatures far above cold crystallization. The common effect of spinning speed on melting of constrained and unconstrained fibers is that the melting peak becomes narrower with increasing spinning speed. In the case of melting peak temperature, the situation is slightly different. In the case of constrained fibers the peak temperature is minimum at moderate spinning speeds (Table 5), while for unconstrained fibers, narrowing of the melting peak is accompanied by formation of a distinct low-temperature shoulder at spinning speeds

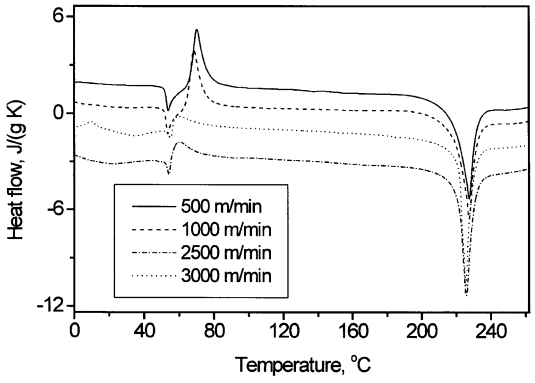

Fig. 3. Differential scanning calorimeter curves from constrained PTT fibers spun at various speeds.

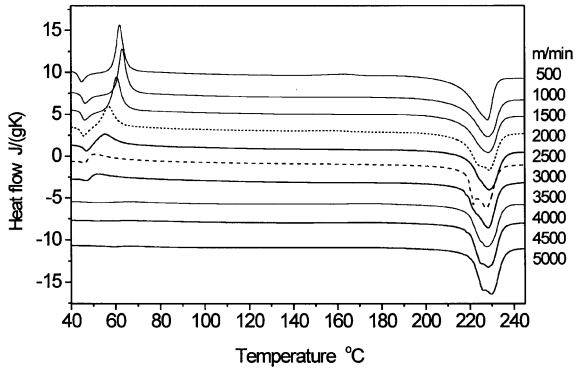

Fig. 4. Differential scanning calorimeter curves from unconstrained PTT fibers spun at various speeds.

Table 5
Melting peak temperature in °C of constrained and unconstrained PTT fibers as function of spinning speed

Spinning speed	Unconstrained fibers		Constrained fibers
	Temperature of the peak of low-temperature shoulder	Temperature of the main peak (higher-temperature peak)	
500	No shoulder	228.2	227.4
1000	No shoulder	228.6	227.3
1500	No shoulder	228.4	227.4
2000	No shoulder	228.9	226.4
2500	223.4	229.0	225.6
3000	221.8	227.6	225.5
3500	224.4	228.3	225.5
4000	225.0	227.8	227.6
4500	225.2	228.3	227.6
5000	225.9	229.8	228.4

above 2500 m/min. The temperature of this shoulder increases with spinning speed, while there is no effect of spinning speed on the peak temperature of the main (high-temperature) peak (Table 5).

4.7. The effect of mechanical constraints during heating

Application of external mechanical constraints during heating shifts the temperature of glass transition and the peak of cold crystallization to higher temperatures. The increase in glass transition temperature is a natural physical consequence of the application of stress resulting from mechanical constraints, while an increase of the temperature of cold crystallization is due to the shift of the glass transition temperature, rather than a direct effect of mechanical constraints. The heat evolved during cold crystallization is independent of mechanical constraints. The only effect on cold crystallization, which can be interpreted as a direct influence of mechanical constraints, is that on the width of the peak of cold crystallization, which is larger for constrained samples than for unconstrained ones.

In the case of melting it is seen that the application of mechanical constraints affects the shape of the melting peak. The melting of the samples with free ends occurs in a relatively broad temperature range and at a spinning speed above 2000 m/min, two separate peaks can be detected. In the case of constrained samples, the low-temperature shoulder is absent (Fig. 5) and the temperature range of melting is narrower.

5. Discussion

It is evident that spinning conditions, especially take-up velocity, determine the structure and thermo-mechanical behavior of as-spun PTT fibers. The behavior of some properties, like shrinkage, appears to be relatively complex. Shrinkage first increases with increasing spinning speed, reaches a maximum and then decreases. Taking into account the relationships presented in Fig. 6, it seems easy to recognize that the initial increase of shrinkage is due to an increase

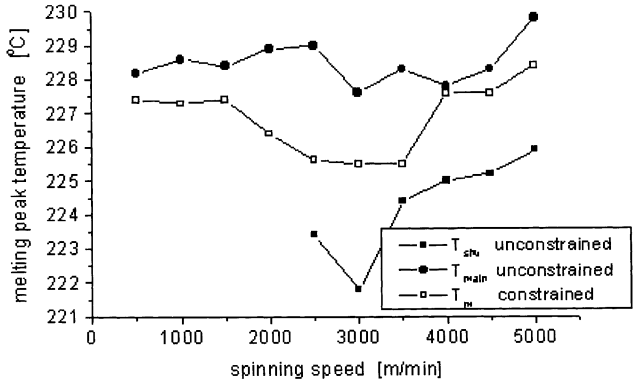

Fig. 5. Melting peak temperatures for constrained and unconstrained fibers.

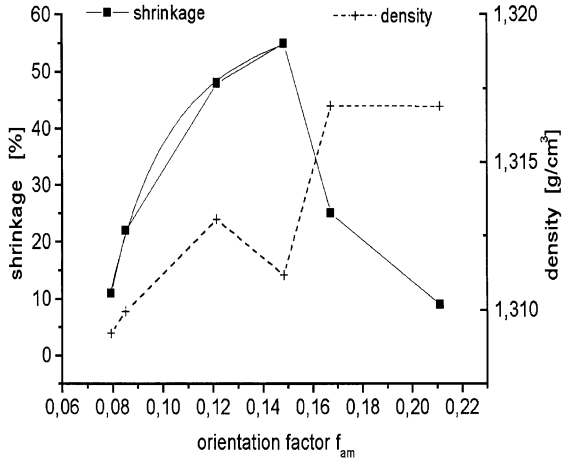

Fig. 6. Shrinkage and density as functions of amorphous orientation factor.

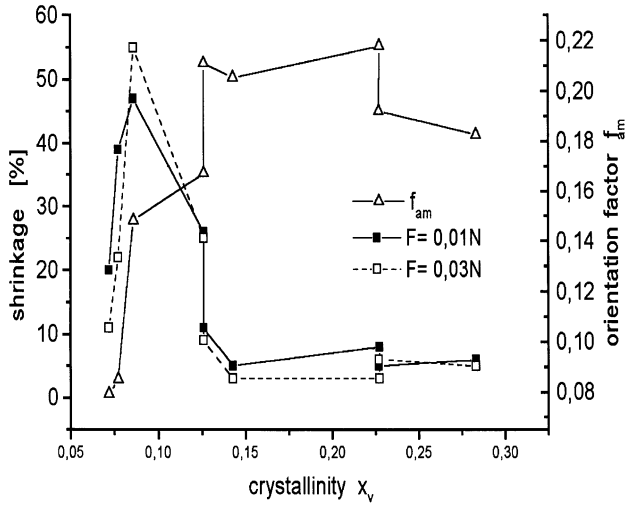

Fig. 7. Shrinkage and amorphous orientation factor as functions of crystallinity.

of amorphous orientation. The increase of shrinkage is observed in the region where density (crystallinity) is still low. When the crystallinity starts to increase, shrinkage is reduced. This means that the presence of crystalline phase in high-speed-spun fibers reduces shrinkage in spite of high amorphous orientation. These conclusions are supported by relationships presented in Fig. 7 where shrinkage and amorphous orientation factors are plotted as functions of crystallinity. It is seen clearly that shrinkage increases very fast with the initial small amount of crystallinity (which accompanies an increase of spinning speed at low speeds), reaches maximum at still very low crystallinity, and abruptly drops when crystallinity increases. The observed thermo-mechanical properties of as-spun PTT fibers can be used for optimizing fiber properties by post-spinning treatment.

References

[1] Ziabicki A, Kawai H, editors. High speed fiber spinning. New York: Interscience, 1985.
[2] Desborough IJ, Hall IH, Neisser JA. Polymer 1979;20:545.
[3] Poulin-Dandurand S, Perez S, Revol JF, Brisse F. Polymer 1979;20:419.
[4] Rappe CJ, Casevit KS, Colwell WA, Goddard III WM, Skiff WM. J Am Chem Soc 1992;114:10,024.
[5] Lyon RE, Farris RJ, MacKnight WJ. J Polym Sci Polym Lett Ed 1983;21(5):323.
[6] Wasiak A, Saijo K, Hashimoto T, Grebowicz J. In preparation.
[7] Sajkiewicz P et al. In preparation.